GAVIN PUBLISHERS

Nanomedicine and Nanoscience Research

Research Article

Liang Q. J Nanomed Nanosci: JNAN-136.

DOI: 10.29011/JNAN-136.100036

Water-Based Route to Controllably Synthesize of Near-Infrared Fluorescent Ag_2S Quantum Dots

Qingshuang Liang*

College of Chemistry and Material Science, Fujian Normal University, China

***Corresponding author:** Qingshuang Liang, College of Chemistry and Material Science, Fujian Normal University, Fuzhou, Fujian 350007, China. Tel: +86059183465156; Email: lqs671@163.com

Citation: Liang Q (2017) Water-Based Route to Controllably Synthesize of Near-Infrared Fluorescent Ag_2S Quantum Dots. J Nanomed Nanosci: JNAN-136. DOI: 10.29011/JNAN-136.100036

Received Date: 01 December, 2017; **Accepted Date:** 14 December, 2017; **Published Date:** 21 December, 2017

Abstract

Since the crystal growth of Ag_2S QDs is very fast due to the extremely low solubility ($K_{sp}=6.3\times10^{-50}$), detailed knowledge of precursor reactions is important to modulate the synthesis process and make the crystal growth more controllable. Lots of parameter, such as ligands, ligand concentration, and precursor concentration, can affect the kinetics of conversion of precursor to monomer. In this work, we describe the preparation of near-infrared luminescent Ag_2S QDs in aqueous solution though a facile one-pot approach at room temperature, and discuss the effect of the ligands, Ag precursor concentration, pH, and molar ratio of ligands: Ag on the kinetics of the precursor reaction. We hope that this work can help the community a deeper understanding of the reaction pathways and the origin of the concentration dependence in the synthesis of Ag_2S QDs, controlling the crystal growth more freewheeling.

Introduction

The important emerging area of whole animal and deep tissue imaging has made Near-Infrared (NIR) imaging of special significance due to their deep tissue penetration and high sensitivity. [1] Over the past years, the development of various kinds of NIR nanomaterials for biological imaging has attracted intense attention. Semiconductor Nanocrystals (NCs) or Quantum Dots (QDs) due to their unique luminescent properties, such as high PL Quantum Yield (QY), broad excitation spectrum, and size-dependent fluorescence properties, have received great interest as biological imaging agents. [2-4] Unfortunately, most of the current developed highly luminescent NIR-QDs, such as CdHgTe [5], Cd_3As_2 [6], Cd_3P_2 [7], CdTe/CdSe [8], and PbS [9], contain highly toxic compounds that limit their applications in biosystems. Recently, ternary I-III-VI_2 NIR QDs ($CuInSe_2$[10], $CuInS_2$[11], and $AgInS_2$[12]) with relatively low toxicity have been synthesized. However, it is tedious and big challenge to tune their ternary composition, which has a significant effect on the optical properties of ternary I-III-VI QDs.

With a band gap of 0.9-1.1 eV and negligible toxicity to organisms, nanoscale α-Ag_2S has been reported as a promising candidate for NIR imaging probes in recent years. [13-18] In 2010, Wang's group reported the first case of NIR fluorescence Ag_2S QDs in the organic phase, but only exhibited one emission maximum at 1050 nm. [13] Pang's group had obtained emission-tunable NIR Ag_2S QDs in rang of 690-1227 nm, and successfully transferred the as-prepared hydrophobic QDs to the aqueous phase via surface ligand exchange. [16] One-pot synthesis of water-dispersible Ag_2S QDs with NIR fluorescence properties has also been reported. [19-22] For example, recently Yan's group had prepared BSA-stabilied NIR Ag_2S QDs in aqueous solution and subsequently bioconjugate the QDs with anti VEGF foe targeted *in vivo* cancer imaging. [20] However, compared to other II-VI semiconductor systems, controllably synthesize Ag_2S nanoparticles is much more difficult. The extremely low solubility of the Ag_2S ($K_{sp}=6.3\times10^{-50}$) generally results in fast crystal growth. [22,23] The synthesis of colloidal semiconductor nanocrystals relies on a chemical reaction between cation and anion precursors. [24] Studies have showed that precursor reactivity dominates the rate of the conversion of precursor to monomer and thus has significant role on the nanocrystals nucleation and growth. [25] Therefore, a deeper understanding of the precursor conversion reactions in the Ag_2S QDs synthesis will clarify productive mechanistic pathways and the origin of the concentration dependence, making the crystal growth more controllable. Here, in this work, we describe the preparation of thioalkyl acid-capped Ag_2S QDs in aqueous solution though a facile one-pot approach at room temperature. These Ag_2S QDs

have ultra-small sizes (3.87±0.4 nm) and exhibits tunable near-infrared luminescent emission from 790 to 824 nm. The effect of a series of react parameter, such as ligands, precursor concentration, pH, and molar ratio of ligands: Ag on the kinetics of the precursor reaction and their influence of the optical properties of as-prepared Ag_2S QDs were discussed. We hope that this work can help the community a deeper understanding of the reaction pathways and the origin of the concentration dependence in the synthesis of Ag_2S QDs, controlling the crystal growth more freewheeling.

Experimental

Materials: All chemicals were used as received without further purification. Silver nitrate ($AgNO_3$) was purchased from Sigma-Aldrich. Mercaptoacetic acid (97%) and 3-mercaptopropionic acids (99%) were obtained from Alfa Aesar. Sulfur powder (99.99%) and 1-thioglycerol (95%) were purchased from Aladdin. Hydrazine (N_2H_4, 50 wt % in H_2O) and isopropanol (analytical grade) were obtained from Beijing chemical works. All of solutions were prepared in distilled water (18.3 M Ω cm^{-1}).

Synthesis of Ag_2S QDs: In a typical reaction, 0.1 M $AgNO_3$ and 0.2 M Thioglycolic Acid (TGA) solution were prepared using distilled water respectively. The S^{2-} source was prepared by dissolving 0.08 g sulfur powder in 7.5 mL of hydrazine hydrate (50 wt %) in open air and stirring at room temperature until it was completely dissolved. 1 mL $AgNO_3$ solution and 7 mL 0.2 M TGA solution were mixed, the pH was adjusted to 6 using NaOH and HNO_3 solution. Then 0.167 mL of the sulfur-hydrazine hydrate solution (0.1 M) was added and a transparent yellow-brown solution was obtained. The mixture was stirred at room temperature for 5 min and the resultant Ag_2S QDs were obtained by precipitated the solution with addition of isopropanol and redispersed in distilled water.

Characterization Methods: UV-visible absorption spectra were recorded on a Cary 50 Scan UV-visible spectrophotometer (Varian, USA). Fluorescence spectra were obtained using a Fluoromax-4 spectro fluorometer (Horiba Jobin Yvon Inc., France). X-Ray Power Diffraction (XRD) patterns were recorded on a D8 Focus diffractometer (Bruker) with a Cu K1 radiation source (λ= 0.15406 nm). The X-Ray Photoelectron Spectroscopy (XPS) measurements were performed on an ESCALAB-MKII 250 photoelectron spectrometer (VG Co.) with $Al_{K\alpha}$ X-ray radiation as the X-ray source for excitation. Infrared spectra were collected on a VERTEX Fourier Transform Infrared (FTIR) spectrometer (Bruker). For the XRD, XPS and FTIR measurements, Ag_2S QDs powders were used, obtained by dying the Ag_2S QDs precipitation in vacuum. Transmission Electron Microscopy (TEM) and High-Resolution Transmission Electron Microscopy (HRTEM) were performed on a FEI Tecnai G2 F20 with an accelerating voltage of 200 kV.

Results and Discussion

Characterization of Ag_2S QDs: The size, morphology and composition of the as-prepared Ag_2S QDs were characterized using High-Resolution Transmission Electron Microscopy (HRTEM), X-Ray Power Diffraction (XRD), X-Ray Photoelectron Spectroscopy (XPS), and Fourier Transform Infrared Spectrometry (FTIR). (Figure 1) shows the typical HRTEM image of the as-prepared TGA-stabilized Ag_2S QDs.

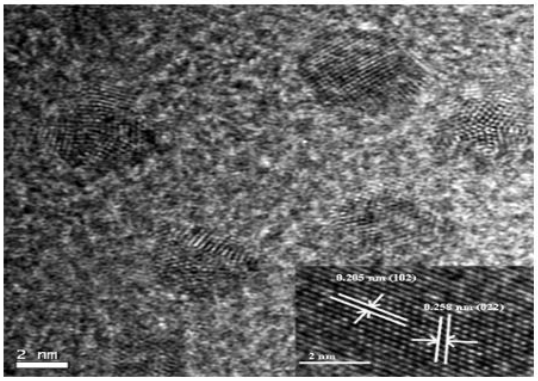

Figure 1: Typical HRTEM image of the as-prepared TGA-stabilized Ag_2S QDs.

The particles were highly dispersible and had obvious lattice planes. The average size of Ag_2S NCs is 3.87±0.4 nm. The lattice planes of the focused nanocrystal with a d-space of 0.205 nm and 0.258 nm could be indexed as the (102) plane and (022) plane of monoclinic Ag_2S nanocrystals. The XRD pattern (Figure 2) of the as-prepared Ag_2S QDs is weak and undistinguishable, similarly to the previous reported [16,21,22].

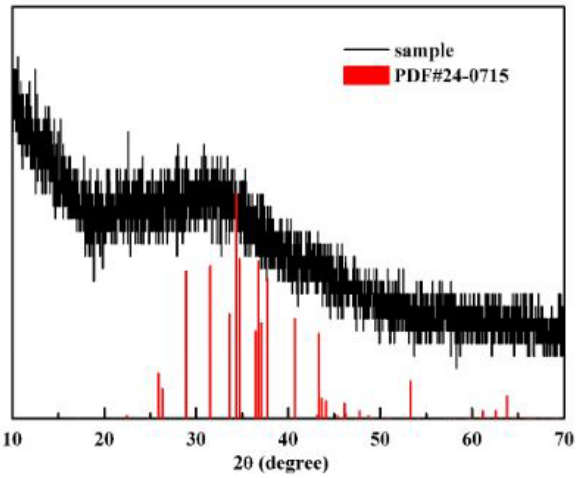

Figure 2: XRD pattern of resultant Ag_2S NCs.

This is possibly because the QDs were too small and coated with plenty of ligands. The XPS results confirmed the chemical composition and chemical status of the as-prepared Ag_2S QDs (Figure 3).

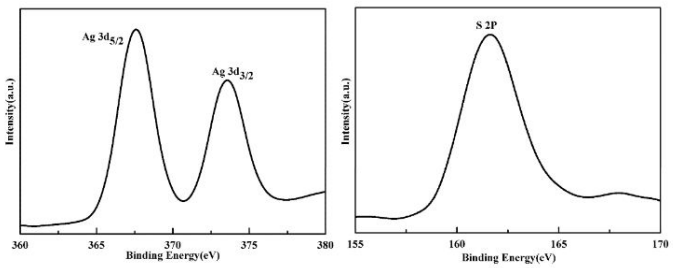

Figure 3: XPS spectra of the as-prepared TGA-stabilized Ag_2S QDs: (a) Ag 3d and (b)S 2P.

The peak at 376.6 and 373.5eV correspond to the Ag $3d_{5/2}$ and $3d_{3/2}$, respectively, indicating that the oxidation state of the Ag ion in the Ag_2S QDs is univalent. The S 2p peak at 161.6eV is assigned to the binding energy of the Ag-S-Ag bond. The actual Ag/S atomic ratio on the QD surface is roughly 1.28:1, indicating that sulfur is slightly excessive. Since the XPS is the surface analyzed technology, this result also indicated that the Ag_2S QDs were coating by TGA. FT-IR spectra of the pure TGA and dried TGA-stabilized Ag_2S QDs are given in (Figure 4).

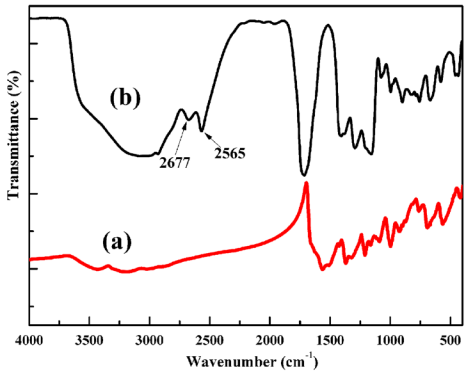

Figure 4(a-b): FI-IR spectra of (a) the obtained TGA-stabilized Ag_2S QDs and (b) the pure TGA.

The acid function of TGA can clearly be identified in (Figure 4b) both through the very broad 3050 cm^{-1} O-H stretching vibration and through the 1702 cm^{-1} C=O stretching vibration. The strong vibration of the carbonyl group of TGA vanished upon surface functionalization of QDs (Figure 4a). The symmetric and asymmetric stretching vibrations of the carboxylate group of the charged TGA appear at 1378 and 1560 cm^{-1}, respectively (Figure 4a). The absence of the SH stretch band between 2677 and 2565 cm^{-1} supports the attachment of the TGA ligand through covalent bonds between thiols and surface Ag atoms of Ag_2S QDs. The spectrum of Ag_2S QDs also displayed the bands assigned to the hydroxyl group of the acid function at 3428 cm^{-1} and of C-H stretching at 2948 cm^{-1}(Figure 4a).

Effect of Reaction Conditions on the as-Prepared Ag_2S QDs: Since the crystal growth of Ag_2S QDs is very fast due to the extremely low solubility ($K_{sp}=6.3\times10^{-50}$), detailed knowledge of precursor reactions is important to modulate the synthesis process and make the crystal growth more controllable. Lots of parameter, such as ligands, ligand concentration, and precursor concentration, can affect the kinetics of conversion of precursor to monomer. Here, we describe the preparation of thioalkyl acid-capped Ag_2S QDs in aqueous solution and discuss the effect of the ligands, Ag precursor concentration, pH, and molar ratio of ligands: Ag on the kinetics of the precursor reaction and the optical properties of as-prepared Ag_2S QDs.

Influence of the Ligand: It is well known that ligands play an important role in the nucleation and growth of nanoparticles. [26] Thioalkyl acids, contained with two functional groups possessing lone pair electron, are widely used as stabilizing and effective size-regulating agents in the II-VI semiconductor nanocrystals synthesis. [27-29] Three common used thiols, Thioglycolic Acid (TGA), 3-Mercaptopropionic Acid (MPA), 1-Thioglycerol (TG), were selected to systematically examine the effect of ligand chemistry on the growth and optical properties of Ag_2S QDs. The temporal evolution of Ag_2S QDs capped with different ligands is shown by the UV-vis absorption spectra in (Figure 5).

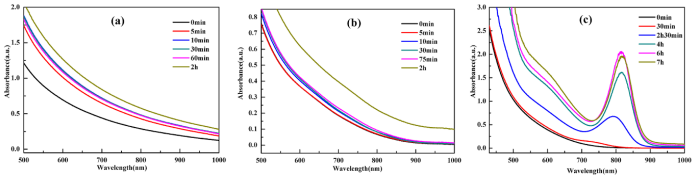

Figure 5(a-c): The temporal evolution of UV-vis absorption spectra of Ag_2S QDs capped with different ligands.

When TG was used as ligand, as shown in (Figure 5a), the absorptions appeared at the beginning of the spectra, indicating the ligands had no size-controlled to the nanoparticles. With MPA as ligand, the absorptions were emerged at the wavelength of 800 nm and slightly red-shifted with increasing growth time as shown in (Figure 5b), suggesting a better size-controlled. Whereas, in the case of TGA as ligand (Figure 5c), the absorptions emerged at 700 nm at first and then a distinct absorption peak at 730 nm was appear after 30min and shifted to longer wavelengths with distinctly for longer growth times. The well-resolved peaks suggest that the as-prepared Ag_2S QDs had high-qualities and narrow size-distributions. As shown in (scheme1), controlling the concentration of Ag^+ is a very effective way to control the kinetics of conversion of precursor to monomer.

$$Ag(L)_n^{2n-1} \rightleftharpoons Ag^+ + nL^{2-}$$

$$2Ag^+ + S^{2-} \longrightarrow (Ag_2S)_i$$

$$(Ag_2S)_i \longrightarrow (Ag_2S)_n$$

$$(Ag_2S)_i + (Ag_2S)_n \longrightarrow (Ag_2S)_m$$

Scheme 1: Precursor conversion to monomer and its subsequent crystallization to nanocrystals. $(Ag_2S)_i$ represents a solvated form of Ag_2S, $(Ag_2S)_n$ represents nucleation, and $(Ag_2S)_m$ represents nanocrystal growth.

Considering that Ag^+ ion is a very soft Lewis acid; soft Lewis base ligands will be more effective as stabilizing agent. According to the principle of Hard and Soft Acids and Bases (HSAB), the degree of softness of the three ligands is TGA>MPA>TG, such the interaction of the TGA ligand to Ag^+ ion is stronger than the other two. The strong binding of TGA ligand to Ag^+ ion result that only a small number of monomers were used in the initial nucleation stage and excess monomers were left for the size-focusing growth. The excess monomers also provide favorable condition for the reconstruction of the surface of nanoparticles, reducing the concentration of surface defects. Using MPA, the monomers were formed immediately after the precursors were injected. The monomers were almost consumed at the nucleation stage and a slow growth fellow, experiencing no surface reconstruction. For the case of TG, the weak binding give rise to quick escape of ligands from the surface of nanoparticles and a rapid growth process. Thus, it was difficult to control the sizes and size distributions of nanoparticles. (Figure 6) shows the PL spectra of Ag_2S QDs stabilized with these three ligands. While the Ag_2S NCs passivated by TG show nearly no PL, nanocrystals coating by TGA exhibit a strong luminescent emission at 812 nm.

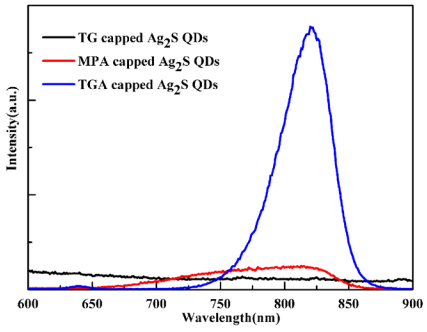

Figure 6: The PL spectra of Ag_2S QDs stabilized with these different ligands.

From the above discussion, we suggest that TGA provides the better surface passivation and controllably synthesize of the Ag_2S QDs under us react conditions. In the fellow discussion, we all used TGA as ligands.

Influence of TGA/Ag Mole Ratio and Solution pH: (Figure 7) shows the UV-vis absorption and PL spectra of Ag_2S QDs prepared under different TGA/Ag^+ mole ratio.

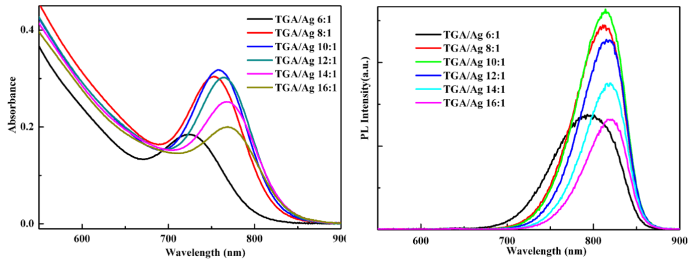

Figure 7: The UV-vis absorption and PL spectra of Ag_2S QDs prepared under different TGA/Ag^+ mole ratio.

As shown, the optical properties of the resulting Ag_2S nanocrystals were dependent on the TGA/Ag^+ mole ratio. With increasing the TGA/Ag^+ mole ratio, a systematic redshift of the absorption peak was observed clearly (from 722 to 770 nm); meanwhile, the PL peak were also found to red shift from 793 to 824 nm. The PL emission initially increased then decreased, and it reached a maximum at the ratio of 10:1. The optical properties of Ag_2S nanocrystals were also found to be influenced by the solution pH shown on (Figure 8).

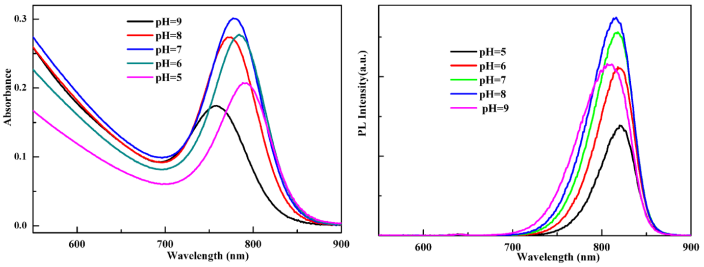

Figure 8: The UV-vis absorption and PL spectra of Ag_2S QDs prepared under different solution pH.

Interestingly, it was noticed that the influences of the TGA/Ag^+ mole ratio and the solution pH on the optical properties of Ag_2S nanoparticles were combined. For example, when the pH is 6, the PL emission reached a maximum at the TGA/Ag^+ mole ratio of 14:1, yet while the pH increases to 8, the PL emission shown the maximum at the ratio of 10:1. It is well known that the ligand/ metal ion mole ratio and the solution pH play important role in the nucleation and growth of nanoparticles. [30,31] Yet how exactly the effect ions were going on has not been reported. We try to elucidate our understanding here. As mentioned in the

above, controlling the concentration of free Ag^+ is a very effective way to control the kinetics of conversion of precursor to monomer, and the free Ag^+ concentration was dominated by the chemical equilibrium of reaction (1) and (2) (scheme1). The TGA/Ag^+ mole ratio and solution pH influenced the concentration of L^{2-} and then the chemical equilibrium of reaction (1), determining the released of free Ag^+ and impacted the rate of monomer generation. When the TGA/Ag^+ mole ratio was low (or the solution pH is high), the relative low L^{2-}concentration promoted the chemical equilibrium of reaction (1) to the right, and a great number of Ag^+ ions were released at the nucleation stage, yielding a high concentration of nuclei and subsequently small size of Ag_2S nanoparticles. While the TGA/Ag^+ mole ratio increased (or the solution pH decreased), the high L^{2-}concentration suppressed the released of free Ag^+, leading to a smaller number of larger-sized Ag_2S QDs.

Influence of Ag Precursor Concentration: The temporal evolutions of both UV-vis absorption and PL spectra of Ag_2S QDs prepared by changing the Ag precursor concentration are shown in figure 9.

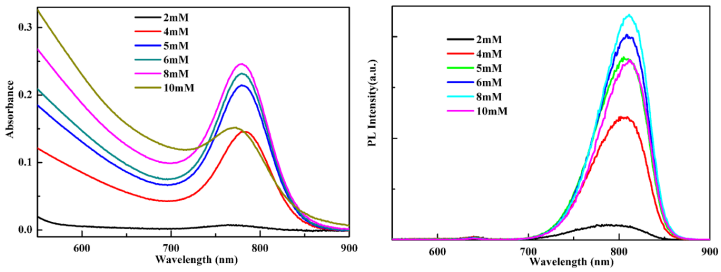

Figure 9: The UV-vis absorption and PL spectra of Ag_2S QDs prepared by changing the Ag precursor concentration.

The photoluminescence was enhanced greatly with the added Ag precursor concentration until 8 mM. Although the PL intensity was found to be strongly dependent on the Ag precursor concentration, less on influence on the absorption and PL position was found. As the TGA/Ag^+ mole ratio and solution pH were keeping constant, the rates of free Ag^+ released were keeping consistent, leading to the same size of the resulting Ag_2S nanoparticles. The change of the Ag precursor concentration will alter the monomer concentration in the solution. Since the appropriate concentration of monomer will provide favorable condition for the reconstruction of the surface of nanocrystals, the PL emission will show the maximum at the optimal Ag precursor concentration.

Conclusion

In this work, we synthesized near-infrared luminescent Ag_2S QDs in aqueous solution though a facile one-pot approach at room temperature. These Ag_2S QDs have ultrasmall sizes (3.87±0.4 nm) and exhibited tunable near-infrared luminescent emission from 790 to 824 nm. Detailed discussion of the influence of the react parameter, such as ligands, precursor concentration, pH, and molar ratio of ligands: Ag on the kinetics of precursor to monomer was performed. Since most of the precursor reactions mechanisms in the nanocrystals synthesis remain unclear, this work may help the community a deeper understanding of the reaction pathways and the origin of the concentration dependence.

Acknowledgements

This work was supported by the National Natural Science Foundation of China under grants no. 20871023, 51002148, 21071141, and 20921002.

References

1. Vikram SH, Pansare J, Faenza WJ, Prud'homme RK (2012) Review of Long-Wavelength Optical and NIR Imaging Materials: Contrast Agents, Fluorophores, and Multifunctional Nano Carriers. Chem Mater 24: 812-827.
2. Louie A (2010) Multimodality Imaging Probes: Design and Challenges. Chem Rev 110: 3146-3195.
3. Lhuillier SKE, Liu H, Sionnest G (2013) Mid-IR Colloidal Nanocrystals. Chem Mater 25: 1272-1282.
4. Aldakov D, Lefrançois A, Reiss R (2013) Ternary and quaternary metal chalcogenide nanocrystals: synthesis, properties and applications. Journal of Materials Chemistry C 1: 3756-3776.
5. n.M.S, Nie S (2011) Bright and Compact Alloyed Quantum Dots with Broadly Tunable Near-Infrared Absorption and Fluorescence Spectra through Mercury Cation Exchange. J AM CHEM SOC 133: 24-26.
6. Harris PMADK, Han HS, Walker BJ, Lee J, Bawendi MG (2012) Synthesis of Cadmium Arsenide Quantum Dots Luminescent in the Infrared. J Am Chem Soc 133: 4676-4679.
7. Xu S, Wilfried-Solo O, Delpech F, Nayral I, Chaudret B (2012) Room-Temperature Synthesis of Air-Stable and Size-Tunable Luminescent ZnS-Coated Cd_3P_2 Nanocrystals with High Quantum Yields. Angew Chem Int Ed 51 (2012) 738 -741.
8. Deng ZT, Nangreave J, Yan H, Liu Y (2012) Robust DNA-Functionalized Core/Shell Quantum Dots with Fluorescent Emission Spanning from UV-vis to Near-IR and Compatible with DNA-Directed Self-Assembly. J AM CHEM SOC 134: 17424-17427.
9. Kershaw SV, Susha AS, Rogach AL (2013) Narrow bandgap colloidal metal chalcogenide quantum dots: Synthetic methods, heterostructures, assemblies, electronic and infrared optical properties. Chemical Society Reviews 42: 3033-3087.
10. Allen PM, Bawendi MG (2008) Ternary I-III-VI Quantum Dots Luminescent in the Red to Near-Infrared. J AM CHEM SOC 130: 9240-9241.
11. Li L, Texier I, Chi TK, Liem NQ, Reiss P (2009) Highly Luminescent $CuInS_2$/ZnS Core/Shell Nanocrystals: Cadmium-Free Quantum Dots for *in vivo* Imaging. Chem Mater 21: 2422-2429.
12. Torimoto T, Tada M, Dai M, Kameyama T, Suzuki S, Kuwabata S (2012) Tunable Photo electrochemical Properties of Chalcopyrite $AgInS_2$ Nanoparticles Size-Controlled with a Photoetching Technique. J Phys Chem C 116: 21895-21902.

13. Xu B, Du YP, Fu T, Cai M, Li F, et al. (2010) Near-Infrared Photoluminescent Ag_2S Quantum Dots from a Single Source Precursor. J AM CHEM SOC 132: 1470-1471.

14. Han L, Lv Y, Asiri AM, Al-Youbi AO, Tu B, et al. (2012) Novel preparation and near-infrared photoluminescence of uniform core-shell silver sulfide nanoparticle@mesoporous silica nanospheres. J Mater Chem 22: 7274-1729.

15. Hong G, Robinson JT, Zhang Y, Diao S, Antaris AL, et al. (2012) *In vivo* Fluorescence Imaging with Ag_2S Quantum Dots in the Second Near-Infrared Region. Angewandte Chemie International Edition 51: 9818-9821.

16. Jiang P, Tian Z, Zhu C, Zhang Z, Pang DW (2012) Emission-Tunable Near-Infrared Ag_2S Quantum Dots Chem. Mater 24: 3-5.

17. Zhang Y, Hong G, Zhang Y, Chen G, Li F, et al. (2012) Ag_2S Quantum Dot: A Bright and Biocompatible Fluorescent Nanoprobe in the Second Near-Infrared Window. ACS NANO 5: 3695-3702.

18. Zhang Y, Zhang Y, Hong G, He W, Zhou K, et al. (2013) Bio distribution, pharmacokinetics and toxicology of Ag_2S near-infrared quantum dots in mice. Biomaterials 34: 3639-3646.

19. Jiang P, Zhu C, Zhang Z, Tian Z, Pang DW (2012) Water-soluble Ag_2S quantum dots for near-infrared fluorescence imaging *in vivo* Biomaterials 33: 5130-5135.

20. Wang Y, Yan XP (2013) Fabrication of vascular endothelial growth factor antibody bio conjugated ultra-small near-infrared fluorescent Ag_2S quantum dots for targeted cancer imaging *in vivo*. Chemical Communications 49: 3324-3326.

21. Hocaoglu I, Çizmeciyan MN, Erdem R, Ozen C, Kurt A, et al. (2012) Development of highly luminescent and cytocompatible near-IR-emitting aqueous Ag_2S quantum dots. J Mater Chem 22: 14674-14681.

22. Wang C, Wang Y, Xu L, Zhang D, Liu M, et al. (2012) Facile Aqueous-Phase Synthesis of Biocompatible and Fluorescent Ag_2S Nanoclusters for Bioimaging: Tunable Photoluminescence from Red to Near Infrared. Small 8: 3137-3142.

23. Yang HY, Zhao YW, Zhang ZY, Xiong HM, Yu SN (2013) One-pot synthesis of water-dispersible Ag_2S quantum dots with bright fluorescent emission in the second near-infrared window. Nanotechnology 24: 055706.

24. Sowers KL, Swartz B, Krauss TD (2013) Chemical Mechanisms of Semiconductor Nanocrystal Synthesis. Chemistry of Materials 25: 1351-1362.

25. Rodriguez RG, Hendricks MP, Cossairt B, Liu H, Owen JS (2013) Conversion Reactions of Cadmium Chalcogenide Nanocrystal Precursors. Chemistry of Materials 25: 1233-1249.

26. Morris-Cohen AJ, Malicki M, Peterson MD, Slavin JWJ, Weiss EA (2013) Chemical, Structural, and Quantitative Analysis of the Ligand Shells of Colloidal Quantum DotsChemistry of Materials 25: 1155-1165.

27. Aboulaich A, Geszke M, Balan L, Ghanbaja J, Medjahdi G, et al. (2010) Water-Based Route to Colloidal Mn-Doped ZnSe and Core/Shell ZnSe/ZnS Quantum Dots. Inorg Chem 49: 10940-10948.

28. Aboulaich A, Balan L, Ghanbaja J, Medjahdi G, Merlin C, et al. (2011) Aqueous Route to Biocompatible ZnSe:Mn/ZnO Core/Shell Quantum Dots Using 1-Thioglycerol As Stabilizer. Chemistry of Materials 23: 3706-3713.

29. Zheng Y, Yang Z, Ying JY (2007) Aqueous Synthesis of Glutathione-Capped ZnSe and Zn1-xCdxSe Alloyed Quantum Dots. Advanced Materials 19: 1475-1479.

30. Shavel A, Gaponik N, Eychmu1ller A (2006) Factors Governing the Quality of Aqueous CdTe Nanocrystals: Calculations and Experiment. J Phys Chem B 110: 19280-19284.

31. Xu S, Wang C, Xu Q, Zhang H, Li R, et al. (2010) Key Roles of Solution pH and Ligands in the Synthesis of Aqueous ZnTe Nanoparticles. Chemistry of Materials 22: 5838-5844.